Smart BPG-Based Lossy Compression of Noisy Grayscale and Color Images

Bogdan Kovalenko [1, *,†], Vladimir Lukin [1,†]

[1] National Aerospace University, 17 Vadyma Man'ka Street, Kharkiv, 61070, Ukraine

Abstract

Compression of imaging data has become a typical operation in image processing chain due to increasing size of acquired images and their number and necessity in transfer image data via communication lines and/or store them. This stimulated special interest to lossy compression techniques able to produce rather large values of compression ratio. However, in practice, a larger compression ratio results in larger distortions introduced into images. Then, a reasonable compromise should be found and provided. The situation becomes even more complex if an image subject to compression, either grayscale or color (three-channel), is noisy. Then, distortions due to lossy compression are introduced to both image content and noise, which occurs to be partly suppressed. In such a situation, one has to solve a task of setting parameter that controls compression (PCC) in a smart (adaptive) manner to reach optimum between positive phenomenon of noise removal and negative fact of information contamination. In this paper, we show how this can be done for a better portable graphics (BPG) coder, which has shown itself to be one of the best modern coders, using a new and efficient quality metrics called HaarPSI able to take into account human visual attention in images. We demonstrate that optimal operation point (OOP) might exist for compressed images according to the metric HaarPSI where probability of OOP existence depends on noise intensity and image complexity. For color images, we show the possibility of OOP existence for all three modes of the BPG coder operation, 4:4:4, 4:2:2, and 4:2:0, where the former mode provides slightly larger HaarPSI values in OOP and the latter mode produces the largest compression ratio. If OOP does not exist (this can be predicted in advance), the recommendations on PCC setting are given. Using test images of different origins and complexity, we demonstrate that the proposed approach to smart lossy compression of noisy images is quite general.

Keywords

Noisy image data, lossy compression, visual quality, intelligent processing

1. Introduction

The amount of images of different origins acquired by various imaging systems rapidly increases nowadays. The obtained images are employed in ecological monitoring, medical diagnostics, non-destructive control, agriculture, mine detection, etc. [1-4]. The acquired images have to be processed, stored, often transferred via communication lines, classified and/or disseminated. In conditions of a limited bandwidth of communication lines and/or memory for image data storage, compression has to be applied to decrease the data size [5-7].

The known methods of compression can be divided into two large groups of lossless [5, 6] and lossy [7] ones. Although there are applications where lossless compression is still used, lossy compression finds more and more applications nowadays. One reason is that lossy compression is able to provide a considerably larger compression ratio (CR) than any lossless technique. Another reason is that CR and quality of compressed images can be varied in wide limits depending on a parameter that controls compression (PCC) for a given coder (e.g., quality factor (QF) for JPEG or bits per pixel (BPP) for JPEG2000). A general tendency in compression of many images is that a larger CR (that corresponds to smaller QF for JPEG and smaller BPP for JPEG2000) leads to larger

ICST-2025: Information Control Systems & Technologies, September 24-26, 2025, Odesa, Ukraine
* Corresponding author.
† These authors contributed equally.
b.kovalenko@khai.edu (B. Kovalenko); v.lukin@khai.edu (V. Lukin)
0000-0002-9360-0691 (B. Kovalenko); 0000-0002-1443-9685 (V. Lukin)

distortions introduced and, thus, worse quality of compressed images according to both traditional metrics, e.g., peak signal-to-noise ratio (PSNR), or visual quality metrics, e.g., feature similarity index measure (FSIM [8]).

The aforementioned tendency is valid for noise-free images for which quality of compressed images becomes worse if CR increases for practically all coders and the task then is to find a proper compromise and to provide it in practice [9-12]. However, it happens quite often that acquired images are noisy, where we mean that noise is visible. There are numerous reasons that noise can be quite intensive: bad conditions of image acquisition [13], principle of image formation [14-16], etc. If an image to be compressed is noisy, its lossy compression might have two specific features [17-19]. The first feature is a specific noise filtering effect due to lossy compression observed for different coders and different types of noise [17-19]. The second feature is possible existence of the so-called optimal operation point (OOP) for which a compressed image is closer (according to a certain metric or similarity measure) to the noise-free (true) image than the original (noisy, uncompressed) image [17-19]. Then, if OOP exists, it is reasonable to compress a given noisy image in OOP neighborhood. If OOP does not exist, a CR smaller than for potential OOP's PCC has to be used [18, 19]. This means that the lossy image compression procedure has to be intelligent, so that it has to take into account various factors (in particular, OOP existence) to provide the best result to meet the user's requirements. This also means that the general approach to lossy compression of images presumes solving a set of particular tasks: 1) What compression method to use? 2) How to get a priori information concerning does OOP exist for a given image to be compressed or no? 3) What PCC value to use if OOP exists, and what should be PCC if OOP does not exist? 4) What metric should be used to characterize image quality? 5) What is the influence of noise type and characteristics on PCC in OOP and how noise type and characteristics can be measured and taken into account?

Then, a complex of studies is needed to answer the aforementioned questions. Not all questions have got answers yet. However, some important answers have been already obtained.

For the case of additive white Gaussian noise (AWGN), the better portable graphics (BPG) coder [20, 21] has recently demonstrated certain benefits compared to both JPEG and modern coders (such as AVIF and HEIF) in the sense of providing a larger PSNR (for compressed image with respect to the corresponding true image) for the same CR in the neighborhood of OOP [22]. The authors of this study have also shown that the BPG coder can perform better than other coders in the situation of complex image compression when OOP is absent; in such cases, the BPG coder produces higher PSNR values for a wide range of CRs. Other advantages of the BPG coder for the considered application is that OOP existence for it can be quite easily and accurately predicted [19] under condition of a priori known noise type and characteristics. Note that methods and algorithms for blind estimation of noise type and characteristics exist nowadays [23, 24]. This allows determining the OOP's PCC Q_{OOP} for the BPG coder for the cases of AWGN and signal-dependent noise [25]. Note that Q_{OOP} for the BPG coder can be determined without any iterative compression/decompression needed for AVIF and HEIF coders. These facts explain our interest to the BPG coder in this paper.

However, not all tasks for lossy compression of noisy images by the BPG coder are solved. The main attention has been previously addressed by us to analysis based on the PSNR metric. Meanwhile, it is known that PSNR is surely not the best metric in characterizing visual quality of compressed images [26]. Visual saliency and the corresponding metrics (for example, HaarPSI) have attracted recent attention of researchers in visual information processing [27, 28]. Thus, in this paper, we analyze performance of the BPG coder for compressing grayscale and color images corrupted by AWGN using the HaarPSI metric. The paper novelty deals just with employing this metric.

2. Image/noise model and compression performance criteria

Performance characteristics of image lossy compression depend on many factors including a used coder, image and noise properties, number of image channels (components), etc. Since performance depends on image complexity, it is nowadays common to analyze a set of images having different

properties (complexity). Taking this into account, in our experiments, we have employed five color images and five grayscale images obtained as intensity images of color ones. Two of them are given in Fig. 1 in color versions. As seen, images are of different origin where the images Lena, Peppers, and Baboon are typical optical test images whilst Frisco and Diego are remote sensing ones. The images Peppers and Frisco are simple structure ones whilst Baboon and Diego are complex structure images.

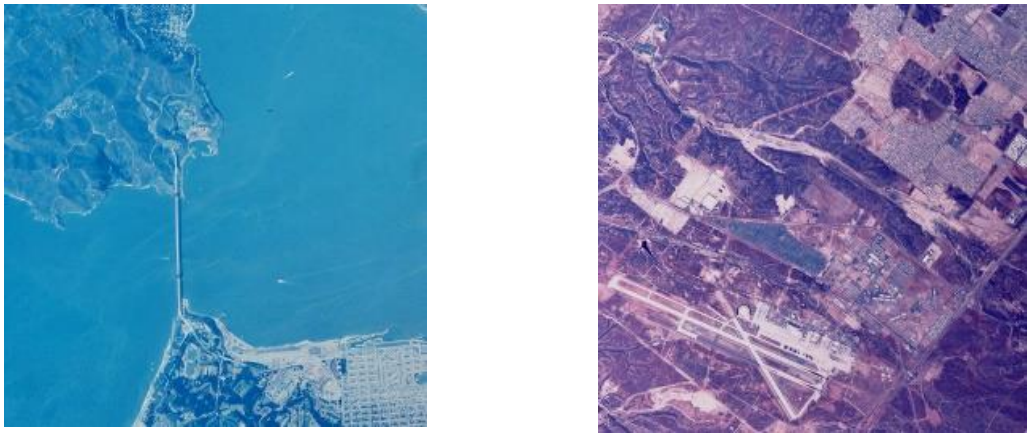

a b

Figure 1: Examples of color images: Frisco (a) and Diego (b).

We assume that the considered test images are corrupted by AWGN with zero mean and variance equal to σ^2. If one deals with color images, noise is supposed to be independent in RGB color components [29]. These are quite typical assumptions, although idealized.

For color image lossy compression, the BPG coder has three modes: 4:4:4 (without color component downsampling), 4:2:2 (set by default), and 4:2:0 (both with color component downsampling). Fig. 2 presents dependencies of CR on Q for two values of σ^2 (64 and 196) for 4:4:4 and 4:2:0 modes. As expected, CR monotonically increases if Q increases. However, there are some peculiarities of behavior for the considered dependencies. First, CR values are quite small if Q<29 for σ^2=64 and if Q<33 for σ^2=196. After this, for larger Q, CR starts to grow quickly. This phenomenon can be explained as follows.

Until the coder does not efficiently filter noise (this happens if Q>29 for σ^2=64 and if Q>33 for σ^2=196), a lot of bits are spent on "noise preservation" since the coder "considers" this noise to be useful information. Another observation is that CR values can differ a lot for the same Q. In particular, this clearly happens for 35≤Q≤40 where CR for simple structure images is larger than CR for complex structure images by several times.

It is also seen that, for Q approaching the upper limit (maximal possible Q equals to 51 for the BPG coder), the CR values are hundreds for any complexity image and any variance of AWGN and compression mode. They are larger for the mode 4:2:0 than for the mode 4:4:4 by a few percent. For small Q, the difference is larger. The results for the 4:2:2 mode are intermediate between the 4:4:4 and 4:2:0 modes.

Consider now the case of lossy compression of the noise-free color images where HaarPSI is calculated between original (noise-free, ideal) and compressed images. Recall that HaarPSI for two identical images is equal to unity and this metric becomes less if images are more dissimilar. Also, differences in two images become visible (noticeable, also treated as just noticeable point (JND) # 1 [30]) if HaarPSI≈0.98. The curves for two modes (4:4:4 and 4:2:0) are presented in Fig. 3.

As seen, all dependences are monotonous and compression effects cannot be visible for Q≤25. All dependencies behave in a very compact manner for Q≤32 and this allows controlling the compressed image visual quality easily for perfect and good quality of compressed data. For Q>32, the dependencies start to diverge where, for the same Q, the visual quality of compressed complex structure images is the worst.

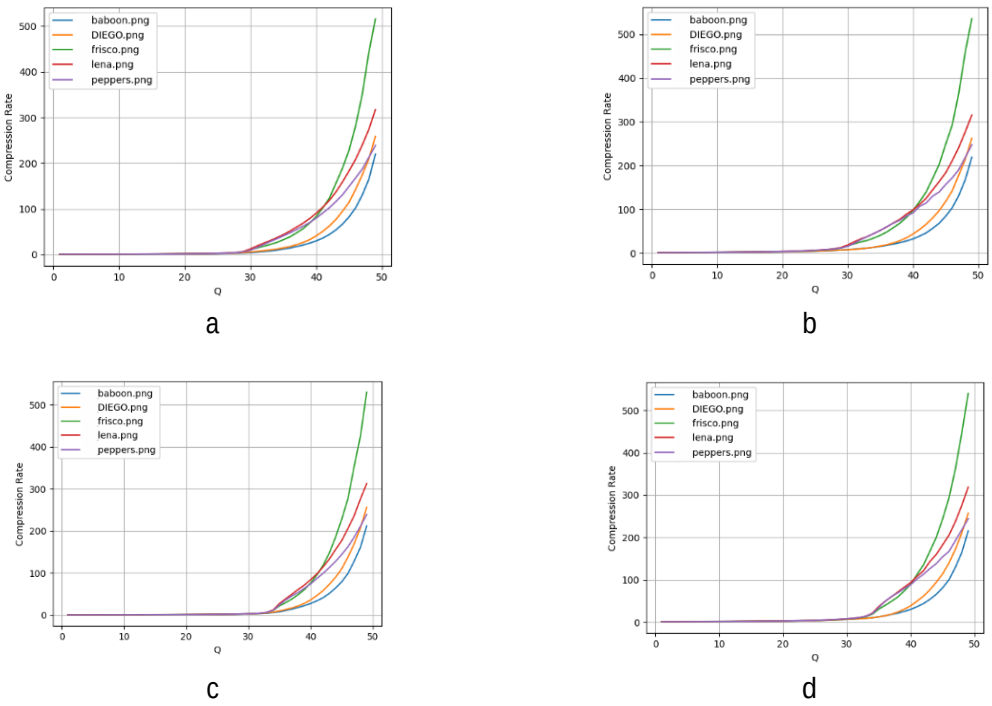

Figure 2: Dependencies of CR on Q for the mode 4:4:4, σ^2=64 (a), 4:2:0, σ^2=64 (b), 4:4:4, σ^2=196 (c), 4:2:0, σ^2=196 (d)

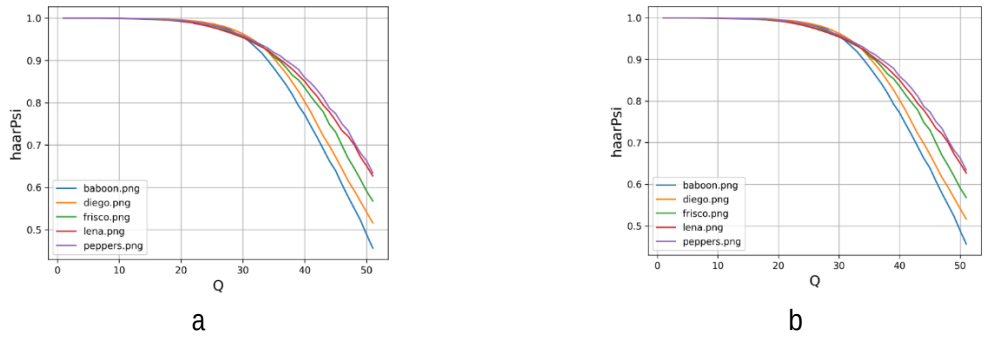

Figure 3: Dependencies HaarPSI on Q for five test color images for 4:4:4 (a) and 4:2:0 (b) modes.

Figures 2 and 3 present two typical dependencies studied for lossy image compression: the dependence of CR on PCC and rate/distortion curves, i.e., dependencies of a metric characterizing image quality on PCC (HaarPSI on Q in the considered case). However, in lossy compression of noisy images, one more type of rate/distortion curves is important – dependencies of a metric calculated between the compressed noisy and noise-free (true) images on PCC. One can argue that in practice it is impossible to calculate such metrics since one does not have true images and only their noisy versions are available. In the next Section, we show that it is possible to obtain such dependencies in simulations by adding noise to noise-free images artificially and then compressing them for different PCC values. Then, knowing the basic properties of such dependences, it becomes clear what to do in practice [18, 19].

3. Lossy compression of noisy images

So, consider the dependencies $HaarPSI_{tc}(Q)$ where the index tc relates to true and compressed. The curves for σ^2=64 are presented in Fig. 4. As seen, there are global maxima of $HaarPSI_{tc}(Q=31)$ observed for all three modes for the image Frisco. This means that, under certain conditions, OOPs can exist. There are also local maxima of $HaarPSI_{tc}(Q=31)$ that take place for the test images Peppers

and Lena. For the complex structure images Baboon and Diego, the dependencies are monotonically decreasing, i.e., OOPs do not exist. Similar phenomena depending image complexity were earlier found for other coders [18] and other quality metrics [19].

For small Q (<28 for the considered σ^2=64), HaarPSI$_{tc}$(Q) practically do not change and they are in the limits from 0.92 to 0.97 depending on image complexity (smaller for simpler structure images). This indicates two phenomena. First, noise is less visible in the complex structure images due to the fact that textures mask the noise. Second, quality of compressed images remains practically the same in a wide range of Q variation since noise filtering effect is negligible and distortions introduced to image content are negligible too. Note that similar effects have been observed in the previous Section for noise-free images.

Let us call Q for which OOP might exist for, at least, one test image as potential Q_{OOP} (later we will show how it can be determined). From analysis of data in Fig. 3, we can state that the main effects are observed in the potential OOP neighborhood, i.e., for Q_{OOP}-3≤Q≤Q_{OOP}+3. For Q>Q_{OOP}+3, image quality rapidly decreases with Q increasing in any case. Thus, our analysis shows that, if Q_{OOP} exists, it is reasonable to compress this image using Q_{OOP}, otherwise, it is expedient to use smaller Q, for example, Q=Q_{OOP}-3 (for complex structure images, this leads to maximal CR provided practically without visual quality reduction). It is interesting that the curve behavior depends on image complexity but not on its origin.

Finally, the results for all three modes are very similar. The only difference is that, for the mode 4:2:0, the values of HaarPSI$_{tc}$ are slightly smaller than for the modes 4:2:2 and 4:4:4.

The observations and rules presented above have been based on the analysis of only one value of noise variance. Then, let us consider the case of σ^2=100. The obtained dependencies are represented in Fig. 5. OOPs are observed again, but in this case they are observed for two out of five test images (Frisco and Lena) and Q_{OOP} shifts towards larger values. Meanwhile, Q_{OOP} is practically the same for both test images for all three modes.

Again, “nothing happens” for Q<Q_{OOP}-3, i.e., quality of compressed images remains practically the same. Similarly, steady degradation of visual quality takes place for Q>Q_{OOP}+3. Local maxima of HaarPSI$_{tc}$(Q) are possible – this time they are observed for the test image Peppers. For complex structure images, Baboon and Diego, the dependencies are still monotonously decreasing and the reasonable practical solution is to set Q=Q_{OOP}-3 or slightly less for compressing such images.

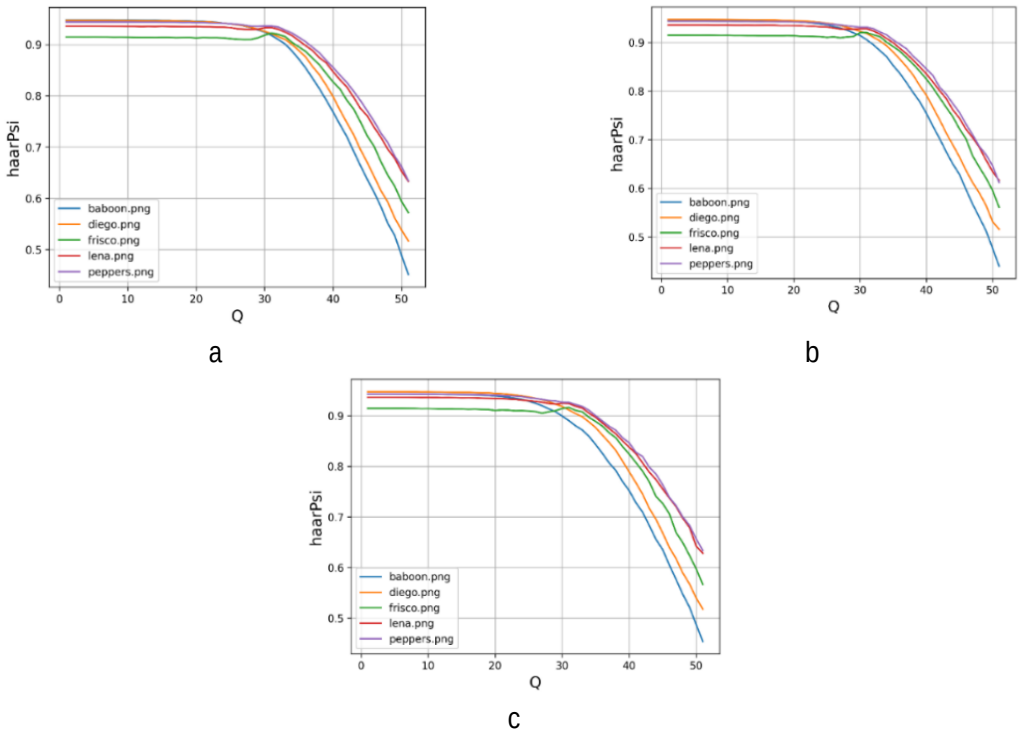

Figure 4: Dependencies of HaarPSI$_{tc}$ on Q for σ^2=64 for the modes 4:4:4 (a), 4:2:2 (b), 4:2:0 (c)

For small Q, $HaarPSI_{tc}(Q)$ are in the limits from 0.88 to 0.92, i.e., their quality is worse than in the previous case (since noise is more intensive and texture masking effect is less). $HaarPSI_{tc}(Q_{OOP})$ are less than 0.98. This means that, even in OOP, the distortions are visible in the lossy compressed noisy images. $HaarPSI_{tc}(Q_{OOP})$ for σ^2=100 are less than $HaarPSI_{tc}(Q_{OOP})$ for σ^2=64, i.e. worse quality of original (noisy) image leads to worse quality of the corresponding compressed image for approximately the same conditions of compression, e.g. for the same Q=20 or for the corresponding potential Q_{OOP}.

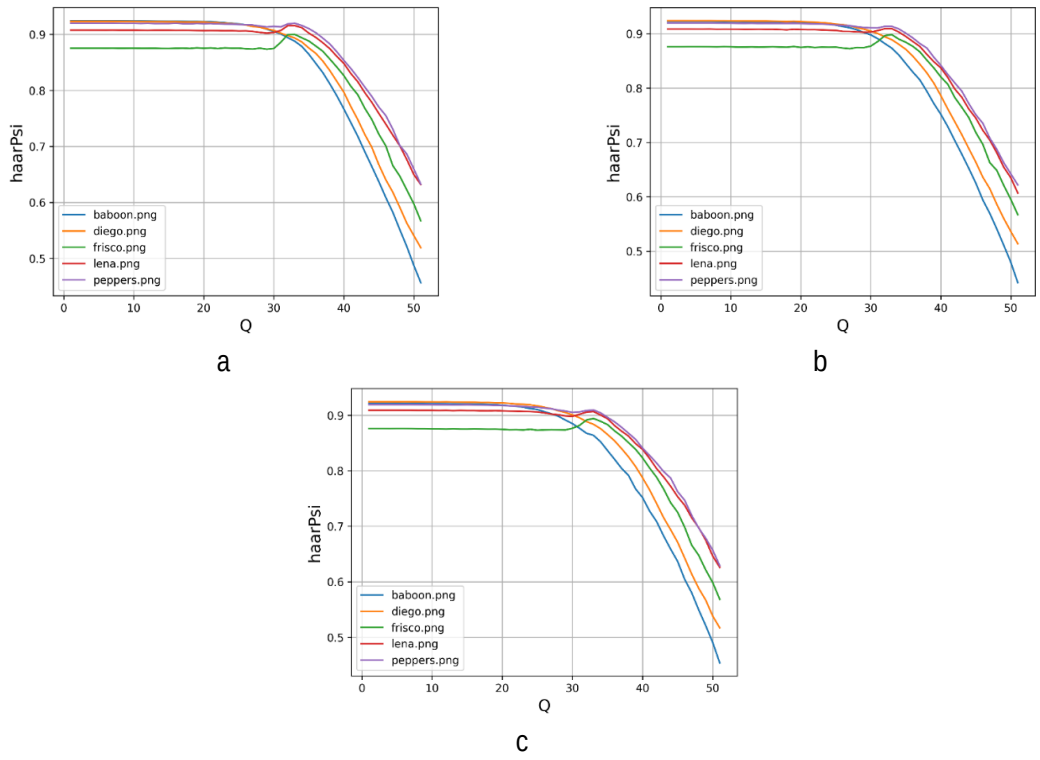

Figure 5: Dependencies of $HaarPSI_{tc}$ on Q for σ^2=100 for the modes 4:4:4 (a), 4:2:2 (b), 4:2:0 (c)

Let us now consider one more value of the noise variance: σ^2=196. The obtained results are presented in Fig. 6. Their analysis shows the following.

First, OOPs are observed for three test images (Frisco, Lena, and Peppers) for all three modes. OOP has shifted to larger values (compared to previous two cases) and now it is observed for $Q_{OOP} \approx 36$. The dependencies for the most complex structure images (Diego and Baboon) still do not have OOP and are monotonically decreasing. Then, it is reasonable to compress the latter two images using $Q=Q_{OOP}-3$ to avoid too large distortions.

Second, for $Q<Q_{OOP}-3$, the compressed image quality almost does not depend on Q (although CR increases if Q increases). For $Q>Q_{OOP}+3$, radical reduction of compressed image quality takes place with Q increasing even if OOP exists. Then, one has to avoid noisy image compression using $Q>Q_{OOP}+3$.

Third, original image quality is not high due to the noise, the quality of compressed images, even if they are compressed in OOP, is such that distortions are clearly visible ($HaarPSI_{tc}$ is smaller than 0.9). Thus, even if the image quality is improved due to lossy compression in OOP, it remains not too high. In other words, the noise in the original image has its negative impact on quality of compressed images. Note that the results for all three modes are, in general, quite similar, although compressed image quality is the worst for the mode 4:2:0 (but this mode provides the largest CR). So, the mode choice depends on priority of requirements to lossy compression – is it more important to provide a better quality or a larger CR. A user can decide what to do for each particular situation.

One positive feature of the BPG-based compression of color noisy images is that, for all images having OOP, this OOP according to the metric HaarPSI is observed for the same Q. Moreover, the

same effect was earlier observed [19] for the metrics PSNR and PSNR-HVS-M. Furthermore, the earlier obtained formula for finding $Q_{OOP}=12.9+20\log_{10}(\sigma)$ is valid for the metric HaarPSI considered in this study. This means that, knowing AWGN σ in advance or having its accurate estimate, one can easily determine the potential Q_{OOP}.

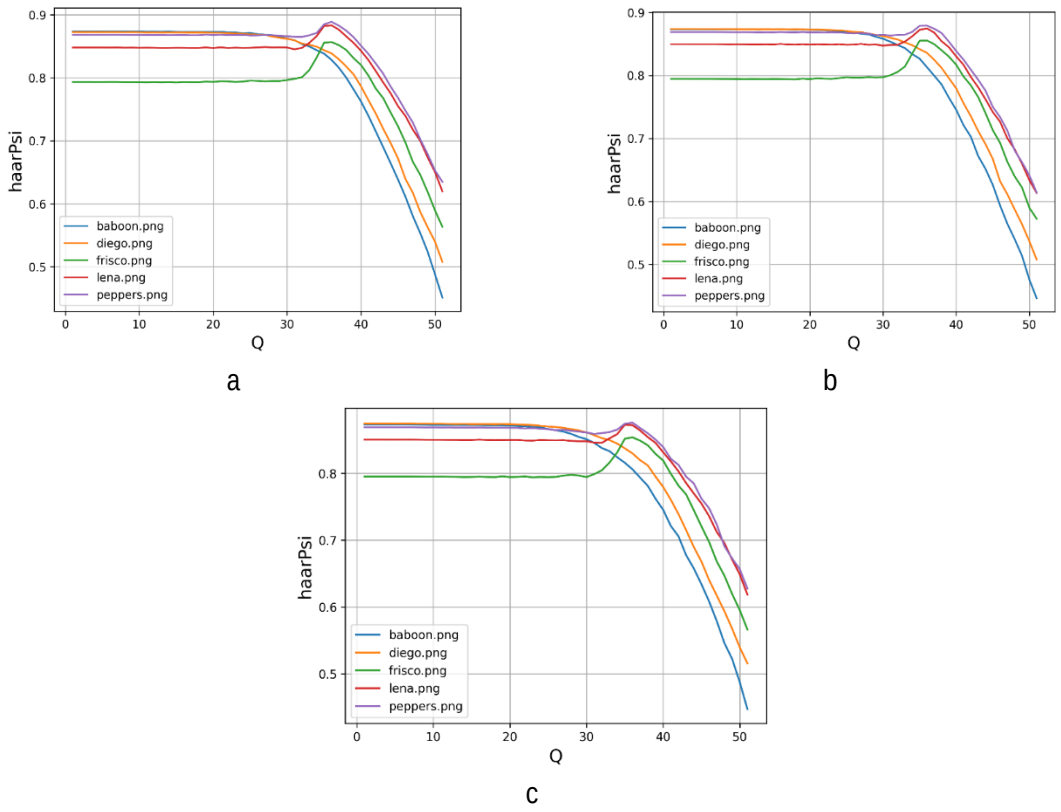

Figure 6: Dependencies of $HaarPSI_{tc}$ on Q for $\sigma^2=196$ for the modes 4:4:4 (a), 4:2:2 (b), 4:2:0 (c)

The presented dependencies and their properties ($Q_{OOP}=12.9+20\log_{10}(\sigma)$) allow formulating the requirements to accuracy of estimation of noise variance or standard deviation if they are not known. To get the estimate of potential Q_{OOP} in the neighborhood [Q_{OOP}-3; Q_{OOP}+3], the estimate of σ_{est} should not differ from its true value σ_{true} by more than 1.4 times ($20\log_{10}(\sigma_{est}/\sigma_{true})\le 3$, $\log_{10}(\sigma_{est}/\sigma_{true})\le 0.15$; $\sigma_{est}/\sigma_{true}\le 10^{0.15}$). We have also analyzed the influence of noise realization on the main characteristics of the rate/distortion curves like those in Figures 4-6. It has been established, e.g., that mean square error of HaarPSI in Q_{OOP} is about 1×10^{-6} for the considered images of the size 512×512 pixels, i.e. noise realization has a very small impact on the main characteristics of rate/distortion curves, at least, for the studied model of AWGN.

One important moment in automation of lossy compression of noisy images is prediction of OOP existence since, if OOP exists, we recommend compressing this image in OOP whilst, if OOP does not exist, we propose to compress the image using $Q=Q_{OOP}$-3. Our studies in [19] have shown that OOP existence can be predicted in advance for PSNR and visual quality metric PSNR-HVS-M. We compared the results for the metrics PSNR-HVS-M and HaarPSI and the conclusions is that, if OOP exists according to PSNR-HVS-M, it also exists for HaarPSI with a very high probability. Then, it is possible to apply the prediction procedure designed for PSNR-HVS-M to predict OOP existence for HaarPSI. Therefore, the automatic smart procedure of lossy compression is the following: 1) estimate AWGN variance if needed; 2) calculate Q_{OOP}; 3) predict OOP existence for this Q_{OOP}; 4) apply compression using Q_{OOP} if, according to prediction, OOP exists or employ $Q=Q_{OOP}$-3, otherwise.

Above, the case of AWGN is considered with identical noise variance in RGB components. In practice, noise can be signal-dependent and/or have not identical characteristics in components of multichannel images. In such situations, it is possible to apply proper variance stabilizing transforms [25, 31, 32] and normalization procedures to reach the additive nature of the noise and its identical

variance in all components. Then, all recommendations on Q setting occur to be valid. The corresponding inverse variance stabilizing transforms have to be carried out after decompression.

4. Lossy compression of grayscale noisy images

In the previous Section, lossy compression of color (three-channel) noisy images has been considered. Meanwhile, an acquired image can be single channel – for example, this can be a single channel synthetic aperture radar (SAR) image [15] or an infrared image. There are also practical situations when several (a few percent) of component images in multispectral or hyperspectral images that are characterized by low input PSNR [14, 18] have to be compressed component-wise with taking into account noise properties whilst other components are compressed without taking noise into account with, possibly, channel grouping.

Thus, peculiarities of single-channel (grayscale) noisy image lossy compression by the corresponding version have to be studied. Note that earlier studies have demonstrated that potential Q_{OOP}, in this case, is approximately equal to $14.9+20\log_{10}(\sigma)$ if the noise is additive white and Gaussian with variance σ^2 for the single-component BPG coder available at [20] for 8-bit image representation. The formula $Q_{OOP}=14.9+20\log_{10}(\sigma)$ was shown to be valid for the metrics PSNR and PSNR-HVS-M. We desire to check whether it is valid for the considered metric HaarPSI. For this purpose, we have used grayscale versions of the five test images used above. Some obtained dependencies are presented in Fig. 7. As seen, similarly to three-component cases, OOP is observed only for one test image for $\sigma^2=64$ (Fig. 7a) and for three test images for $\sigma^2=196$. Local maxima of dependencies $\text{HaarPSI}_{tc}(Q)$ are observed in some cases. The dependencies for complex structure images are monotonically decreasing.

If noise variance increases, Q_{OOP} shifts towards larger values, and the formula $Q_{OOP}\approx 14.9+20\log_{10}(\sigma)$ is valid for the metric HaarPSI. The difference for color and grayscale cases in formulas for determination of Q_{OOP} is explained by the fact that the color system conversion from RGB to YCbCr is carried out for the three-channel case before component-wise compression of decorrelated data. Such a conversion changes noise variance (it is smaller in Y, Cb, and Cr components than originally in R, G, and B components).

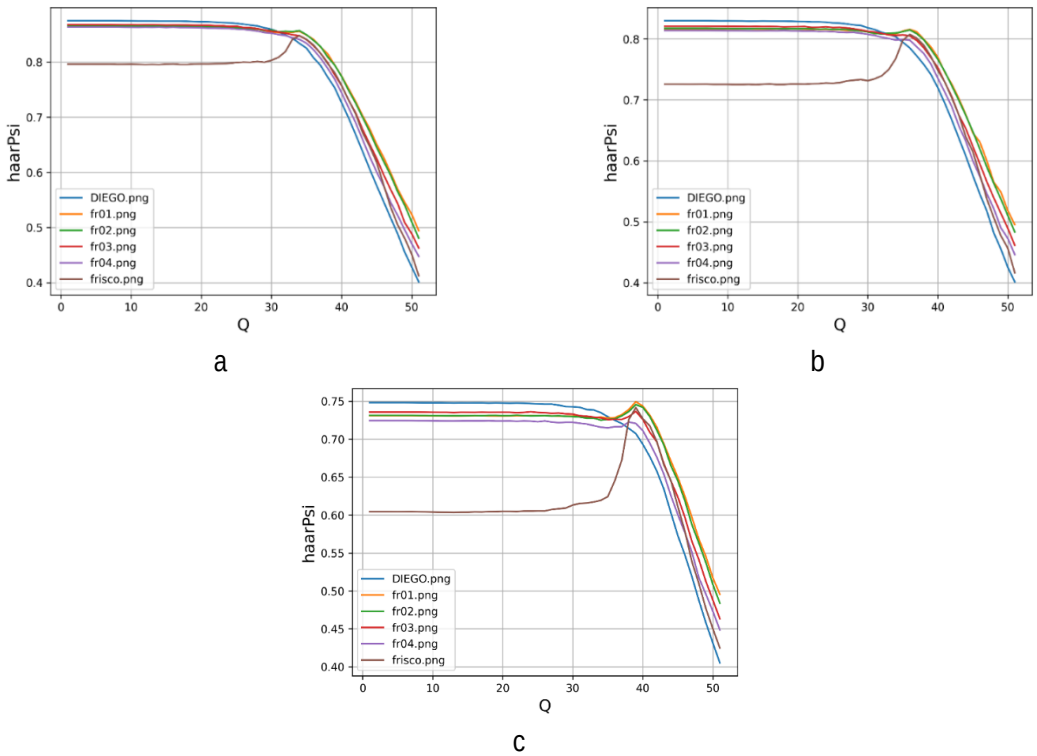

Figure 7: Dependencies of HaarPSI_{tc} on Q for grayscale images for $\sigma^2=64$ (a), $\sigma 2=100$ (b), $\sigma^2=196$ (c)

If noise is not additive in grayscale images, variance stabilizing and normalizing transforms can be applied before compression [25] and inverse transforms should be used after decompression. This has been successfully tested for Poisson noise [25] but has not yet been tested for other types of signal-dependent noise.

5. Some examples

Let us present some examples. First of all, Fig. 8a presents the noisy color image Peppers, where noise is clearly visible in practically all fragments of this image since its intensity is high (σ^2=196). The compressed images obtained for $Q=Q_{OOP}$=36 for the modes 4:4:4 (Fig. 8b), 4:2:2 (Fig. 8c) and 4:2:0 (Fig. 8d) show that the noise is suppressed considerably. The edges and details are preserved quite well although some distortions that appear due to both noise in original image and its lossy compression are visible as well. Visual comparison also indicates that the images compressed for the three studied modes look quite similarly and have approximately the same visual quality.

Fig. 9a represents the noisy grayscale image with the same noise variance (σ^2=196). Noise is seen well and it seems even more intensive than in color image (Fig. 8a). The image compressed in OOP (in this case $Q=Q_{OOP}$=39) is presented in Fig. 9b. Again, the noise is suppressed well while details and edges are preserved well enough. Specific (not annoying) artifacts can be noticed. This shows that for the considered case of very intensive noise the joint impact of the noise in original image and its lossy compression leads to certain negative outcomes. But the positive effects of noise suppression and attaining quite large CR evidence in favor of lossy compression of noisy images in OOP. A similar example for the image Frisco is given in Fig. 10 where Fig. 10a shows the noisy image and Fig. 10b presents the image compressed in OOP. Good noise suppression is observed although some smearing and artifacts are introduced.

a b c d

Figure 8: Noisy color image with σ^2=196 (a) and compressed image (Q=36) for the modes 4:4:4 (b), 4:2:2 (c), 4:2:0 (d)

a b

Figure 9: Noisy grayscale image with σ^2=196(a) and compressed image (Q=39) (b)

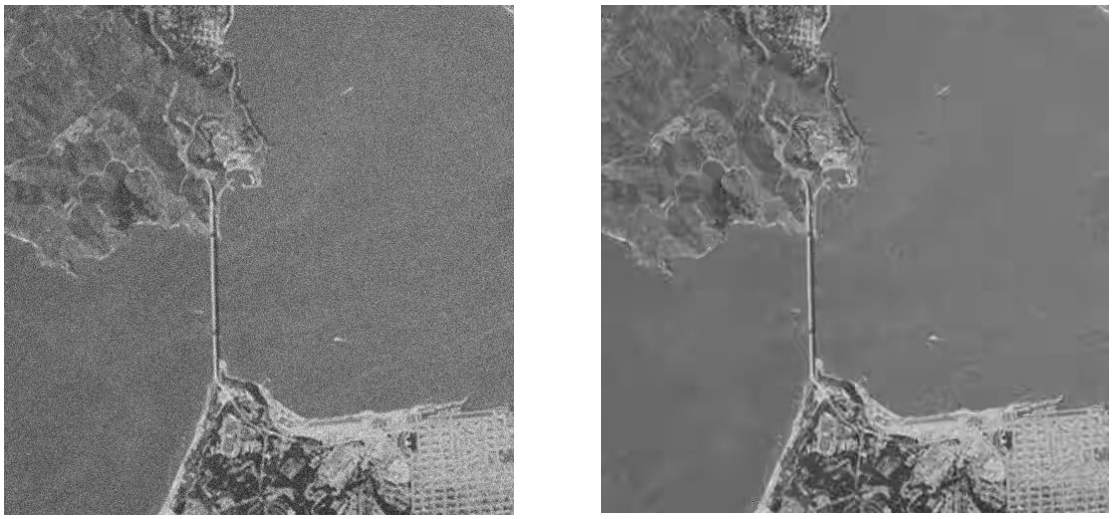

a b

Figure 10: Noisy grayscale image Frisco with σ^2=196(a) and compressed image (Q=39) (b)

6. Conclusions and future work

We have demonstrated that OOP is possible according to the visual attention metric HaarPSI for noisy color and grayscale images compressed by the BPG coder. Obvious advantages of this coder are the following: 1) for a given AWGN variance, OOP (if it exists) is observed for the same Q_{OOP} for all images and all adequate metrics including HaarPSI that simplifies setting the recommended Q for practical situations; 2) OOP existence is more probable for more intensive noise and less complex images; OOP existence can be predicted in advance for known or accurately pre-estimated AWGN variance; 3) this allows automatic setting of Q for a given noisy image according to the offered recommendations and the proposed procedure; 4) CR for simpler structure images is usually considerably larger for simpler structure images although it also depends on noise intensity; 5) the procedures for signal-dependent noise are proposed that allow taking noise characteristics into account; 6) the main observations are general meaning that they do not depend on origin of an image to be compressed; for optical and remote sensing images the main dependencies are on image complexity and noise intensity. The obtained results can be used to develop intelligent lossy compression methods that can compute image parameters and use them to predict OOP or quality metrics to automatically configure and adjust the PCC parameter according to the requirements.

In the future, we plan to analyze the cases of spatially correlated noise and other than Poisson types of signal-dependent noise typical for SAR and ultrasound images. The research has been

funded by National Research Foundation of Ukraine (https://nrfu.org.ua/en/, accessed on 11 July 2025) within Project No. 2023. 04/0039 "Geospatial monitoring system for the war impact on the agriculture of Ukraine based on satellite data" (2024–2025).

Declaration on Generative AI

The authors have not employed any Generative AI tools.

References

[1] J. Jiang, K. Johansen, Y.-H. Tu, M. F. McCabe, Multi-sensor and multi-platform consistency and interoperability between UAV, Planet CubeSat, Sentinel-2, and Landsat reflectance data, GIScience & Remote Sensing 59:1 (2022) 936–958. doi:10.1080/15481603.2022.2083791.

[2] W. Xu, Y. Fu, D. Zhu, ResNet and its application to medical image processing: Research progress and challenges, Computer Methods and Programs in Biomedicine, volume 240, 2023, doi: 10.1016/j.cmpb.2023.107660.

[3] E. Alvarez-Vanhard, T. Corpetti, T. Houet, UAV & satellite synergies for optical remote sensing applications: A literature review, Science of Remote Sensing 3 (2021) 100019. doi:10.1016/j.srs.2021.100019.

[4] Z. Huang, D. Chen, C. Zhong, Few-Shot Object Detection for Remote Sensing Images via Pseudo-Sample Generation and Feature Enhancement. Applied Sciences 15(8) (2025) 4477. doi: 10.3390/app15084477.

[5] Z. Liu, S. Wang and Y. Gu, SAR Image Compression With Inherent Denoising Capability Through Knowledge Distillation, in IEEE Geoscience and Remote Sensing Letters, volume 21, 2024, pp. 1-5, Art no. 4008005, doi: 10.1109/LGRS.2024.3386758.

[6] K. Chow, D. Tzamarias, I. Blanes, J. Serra-Sagristà, Using Predictive and Differential Methods with K2-Raster Compact Data Structure for Hyperspectral Image Lossless Compression, Remote Sensing 11 (2019) 2461. doi:10.3390/rs11212461.

[7] L. Santos, S. Lopez, G.M. Callico, J.F. Lopez, R. Sarmiento, Performance Evaluation of the H.264/AVC Video Coding Standard for Lossy Hyperspectral Image Compression, IEEE Journal of Selected Topics in Applied Earth Observations and Remote Sensing 5 (2012) 451–461, doi:10.1109/JSTARS.2011.2173906.

[8] L. Zhang, L. Zhang, X. Mou, D. Zhang, FSIM: A Feature Similarity Index for Image Quality Assessment, IEEE Trans. Image Processing, vol. 20, no. 8, 2011, pp. 2378-2386. doi: 10.1109/TIP.2011.2109730.

[9] E. Christophe, Hyperspectral Data Compression Tradeoff, in: S. Prasad, L. Bruce, J. Chanussot, (eds.) Optical Remote Sensing. Augmented Vision and Reality, volume 3. Springer, Berlin, Heidelberg, 2011, pp. 9–29. doi: 10.1007/978-3-642-14212-3_2.

[10] S. Cai, X. Liang, S. Cao, L. Yan, S. Zhong, L. Chen, X. Zou, Powerful lossy compression for noisy images, in: 2024 IEEE International Conference on Multimedia and Expo (2024) pp. 1-6. doi: 10.48550/arXiv.2403.14135.

[11] B. Jähne, Almost lossless compression of noisy images. Technisches Messen, 90 (7-8) (2023) 454-463. doi: 10.1515/teme-2023-0028.

[12] Y. Blau, T. Michaeli, Rethinking Lossy Compression: The Rate-Distortion-Perception Tradeoff, in: Proc. 36th International Conference on Machine Learning, volume 97, 2019, 675-685. doi: 10.48550/arXiv.1901.0782.

[13] W. Wang, X, Zhong, Z. Su, On-Orbit Signal-to-Noise Ratio Test Method for Night-Light Camera in Luojia 1-01 Satellite Based on Time-Sequence Imagery, Sensors 19 (2019) 4077, doi:10.3390/s19194077.

[14] P. Zhong, R. Wang, Multiple-Spectral-Band CRFs for Denoising Junk Bands of Hyperspectral Imagery, IEEE Transactions on Geoscience and Remote Sensing 51(4) (2013) 2260–2275, doi:10.1109/TGRS.2012.2209656.

[15] A.G. Mullissa, C. Persello, V. Tolpekin, Fully Convolutional Networks for Multi-Temporal SAR Image Classification, in: Proc. IGARSS 2018 - 2018 IEEE International Geoscience and Remote Sensing Symposium, Valencia, Spain, 2018, pp. 6635–6638. doi: 10.1109/IGARSS.2018.8518780.
[16] A. Ramirez-Jaime, K. Pena-Pena, G. R. Arce, D. Harding, M. Stephen, J. MacKinnon, HyperHeight LiDAR Compressive Sampling and Machine Learning Reconstruction of Forested Landscapes, in: IEEE Transactions on Geoscience and Remote Sensing, vol. 62, 2024, pp. 1-16, Art no. 4402416. doi: 10.1109/TGRS.2024.3356389.
[17] O.K. Al-Shaykh, R.M. Mersereau, Lossy Compression of Noisy Images, in: IEEE Transactions on Image Processing, volume 7, no. 12, 1998, pp. 1641-1652. doi: 10.1109/83.730376.
[18] A.N. Zemliachenko, S.K. Abramov, V.V. Lukin, B. Vozel, K. Chehdi, Lossy Compression of Noisy Remote Sensing Images with Prediction of Optimal Operation Point Existence and Parameters, Journal of Applied Remote Sensing 9(1) (2015) 095066. doi:10.1117/1.JRS.9.095066.
[19] B. Kovalenko, V. Lukin, B. Vozel, BPG-Based Lossy Compression of Three-channel Noisy Images with Prediction of Optimal Operation Existence and Its Parameters, Remote Sensing 15(6) (2023) 1669. doi: 10.3390/rs15061669.
[20] Fabrice Bellard, BPG Image Format, 2018. URL: https://bellard.org/bpg/.
[21] D. Yee, S. Soltaninejad, D. Hazarika, G. Mbuyi, R. Barnwal, A. Basu, Medical Image Compression Based on Region of Interest Using Better Portable Graphics (BPG), in: Proc. 2017 IEEE International Conference on Systems, Man, and Cybernetics (SMC), Banff, AB, Canada, 2017, pp. 216-221, doi: 10.1109/SMC.2017.8122605.
[22] S. Kryvenko, V. Lukin, B. Vozel, Lossy Compression of Single-channel Noisy Images by Modern Coders. Remote Sensing 16(12) (2024) 2093. doi: 10.3390/rs16122093.
[23] M. Colom, A. Buades, J.-M. Morel, Nonparametric Noise Estimation Method for Raw Images. Journal of the Optical Society of America A 31(4) (2014) 863–871. doi:10.1364/JOSAA.31.000863.
[24] V. Abramova, S. Abramov, K. Abramov, B. Vozel, Blind Evaluation of Noise Characteristics in Multichannel Images, in: M. Nechyporuk, V. Pavlikov, D. Krytskyi, (eds.) Information Technologies in the Design of Aerospace Engineering. Studies in Systems, Decision and Control, Springer, Cham, volume 507, 2024, pp. 209–229. doi:10.1007/978-3-031-43579-9_4
[25] V. Naumenko, B. Kovalenko, V. Lukin, BPG-based compression analysis of Poisson-noisy medical images, Radioelectronic and computer systems 3(107) (2023) 91–100. doi: 10.32620/reks.2023.3.08.
[26] W. Lin, C.-C.J. Kuo, Perceptual visual quality metrics: A survey, Journal of Visual Communication and Image Representation 22(4) (2011) 297-312. doi:10.1016/j.jvcir.2011.01.005.
[27] R. Reisenhofer, S. Bosse, G. Kutyniok, T. Wiegand, A Haar Wavelet-Based Perceptual Similarity Index for Image Quality Assessment, Signal Processing: Image Communication 61 (2018), 33-43. doi:10.1016/j.image.2017.11.001
[28] L. Li, T. Xu, Y. Chen, Fuzzy Classification of High Resolution Remote Sensing Scenes Using Visual Attention Features, Comput Intell Neurosci 2017 (2017) 9858531. doi: 10.1155/2017/9858531.
[29] Color Image Processing: Methods and Applications, R. Lukac, K.N. Plataniotis, (eds.), Image processing series; CRC Press/Taylor & Francis: Boca Raton, 2007. doi: 10.1201/9781315221526.
[30] B. Bondžulić, N. Stojanović, V. Petrović, B. Pavlović, Z. Miličević, Efficient Prediction of the First Just Noticeable Difference Point for JPEG Compressed Images, Acta Polytechnica Hungarica 18(8) (2021) 201-220. doi:10.12700/APH.18.8.2021.8.11.
[31] D. Kipele and K. A. Greyson, Poisson Noise Reduction with Nonlocal-PCA Hybrid Model in Medical X-ray Images, Journal of Image and Graphics, Vol. 11, No. 2, 2023, pp. 178-184. doi: 10.18178/joig.11.2.178-184
[32] N. H. Hai, D. N. H. Thanh, N. N. Hien, C. Premachandra and V. B. S. Prasath, A Fast Denoising Algorithm for X-Ray Images with Variance Stabilizing Transform, 2019 11th International Conference on Knowledge and Systems Engineering (KSE), Da Nang, Vietnam, 2019, pp. 1-5, doi: 10.1109/KSE.2019.8919364.